# Continuous waves generated by focused radiators

Ernest L. Madsen, Mitchell M. Goodsitt, and James A. Zagzebski

*Medical Physics Department, University of Wisconsin, Madison, Wisconsin 53706*
(Received 24 May 1981; accepted for publication 1 August 1981)

A single integration technique for calculating the pressure distribution in the field of a focused sinusoidally oscillating radiator is described. This technique involves the direct closed form integration of one of the integrals in the Rayleigh formula; the latter formula itself contains a double integral corresponding to integration over the area of the source transducer face. Precise experimental measurements of a hydrophone's response to the pressure field generated by a focused medical diagnostic transducer are also reported, and comparison between experiment and theory is made. Very good agreement between theory and experiment is demonstrated with respect to both amplitude and phase for lateral beam profiles at six different distances from the source transducer. At a seventh distance (about 1 cm from the source transducer) much more violent fluctuations in the response are observed than result from the theory.

PACS numbers: 43.20.Rz, 43.20.Bi

## INTRODUCTION

The pressure field distribution for a flat circular piston type (nonfocused) radiator, executing steady-state sinusoidal oscillations, can be found by direct integration of the Rayleigh formula over the area of the transducer face. Impulse-response techniques, involving Green's functions in the time domain, have been employed[1,2] to reduce the number of integrations to one—an important simplification regarding computer time costs. For a focused radiator Kossoff[3] agrees with O'Neil's[4] statement that "the general expression for the off-axis intensity distribution is complicated and requires the evaluation of a double integral." This perhaps overlooks the work of Penttinen and Luukkala[5] in which impulse-response methods are used in reducing the double integral to a single one for a focused radiator. The latter authors' approach involves time dependent Green's functions in the manner of Lockwood and Willette.[2]

O'Neil[4] points out and Penttinen and Luukkala reiterate, that the Rayleigh formula is rigorously correct for planar ultrasonic radiators in an infinite rigid baffle, but that for spherical focused transducers this formula is an approximation due to secondary diffraction effects. They state that the approximation is a very good one, however, if the radius of the transducer is large compared to the wavelength.

In the first part of the present paper a derivation of the pressure field due to a sinusoidally oscillating focused radiator is presented as an alternative to that of Pentinnen and Luukkala. The pressure field again is expressed in the form of a single integral. The pressure field is obtained by approaching the Rayleigh formula directly and performing one of the spatial integrations exactly leaving a single integration to be done numerically. There is no excursion into the time domain as in the impulse-response theory. Although the theoretical results are presumably equivalent to those of Penttinen and Luukkala, the derivation presented here possesses, for some readers, the didactic advantage of avoiding the "Green's function" methodology. The important—or perhaps elusive—points of derivation are outlined.

Careful experimental measurements of amplitudes and phases of a hydrophone's response to continuous wave (cw) bursts generated with a focused transducer were also made along lines perpendicular to the beam axis at seven different locations along the beam axis. These seven locations span the region for which the transducer would be used diagnostically. These measurements are reported in the second part of this work. Probably the most important aspect of this work is the direct comparison of the theory with these experimental measurements.

Later in the paper (Sec. IV) a method is presented in which a short duration pulse beam can be theoretically expressed as a linear superposition of continuous wave beams; also included is how to account for attenuation and dispersion in the transmitting medium. This method is employed in the theory section of a companion paper on pressure field patterns of a pulsed focused transducer in attenuating and nonattenuating media.[6]

## I. DERIVATION OF THE PRESSURE FIELD

The solution is defined for two regions separated by the cone-shaped surfaces formed by lines passing from the edge of the spherical transducer through the center of curvature. We refer to the region inside the cone-shaped surface as region I and the remainder as region II (see Fig. 1 in which region I is shaded). Region I includes the axis of symmetry and consists of two parts: a finite volume to the left of the center of curvature and an infinite volume to the right. Region II includes the remaining volume to the right of the circular ring defining the boundary of the radiating element and also to the right of the surface of a large-angle cone, $B$, which is tangent to the radiating element at its circular boundary.

Again referring to Fig. 1, we call the projected radius of the transducer $a$ and its radius of curvature $A$. Let us place the origin of a Cartesian coordinate system at the center of curvature, the $h$ axis being along the axis of symmetry, as shown, and the $x$ axis perpendicular to the $h$ axis and in the plane of the figure. Due to cylindrical symmetry of the solution, we need only find the pressure at all points in the $x,h$ plane for $x \geq 0$. We take $h > 0$ for points to the right of the plane perpendicular to the axis of symmetry and passing through the center of curvature and $h < 0$ *for points to*

 0001-4966/81/111508-10$00.80  

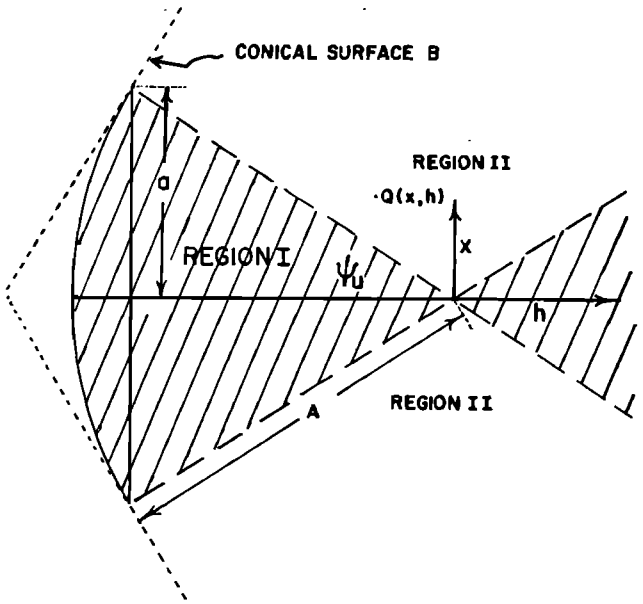


FIG. 1. Diagram showing the division of the focused transducer field into regions I and II. Region I is shaded. The axis of symmetry of the radiating element lies on the horizontal line in the figure. The radius of curvature of the radiating element is $A$, and the circle defining the outer edge of the radiating element is $a$.

*the left* of this plane. The value of $x$ is positive for points above the axis of symmetry and negative for points below. The point $Q(x,h)$ in the figure is in region II with $x>0$ and $h<0$. Notice that the angle $\psi_u$ defining the conical surface separating regions I and II is given by $\psi_u=\sin^{-1}(a/A)$. The velocity potential is

$$\Psi(x,h)=\int_S \frac{u}{2\pi r'}\, e^{ikr'}\, da',$$

where $k$ is the wavenumber, a real number if the transmitting medium is not attenuating. As in Morse and Ingard,[7] we choose the + sign in the exponential instead of minus ($e^{ikr'}$ instead of $e^{-ikr'}$ as in O'Neil[4]). $u$ is the normal component of the velocity at the surface of the radiator, and for outgoing sinusoidal waves, is proportional to $e^{-i\omega t}$, $\omega$ being the angular frequency. We define $u_0$ to be the (real, positive) amplitude of $u$:

$$u=u_0e^{-i\omega t}, \quad \text{for } u_0>0.$$

$da'$ is the surface area element, $S$ is the area defining the radiating surface, and $r'$ is the distance from a point at which $da'$ is found to the field point [such as $Q(x,h)$ in Fig. 1]. The pressure $p(x,h)$ at some point $Q(x,h)$ is then given by

$$p(x,h)=\mathrm{Re}\left(\rho\frac{\partial\Psi}{\partial t}\right),$$

where $\rho$ is the density and Re means "real part of." We have

$$\frac{\partial\Psi}{\partial t}=-i\omega\Psi;$$

thus we have

$$p=\mathrm{Re}(-i\omega\rho\Psi).$$

We define the complex differential quantity $dp$:

$$dp\equiv\frac{-i\omega\rho u}{2\pi}\frac{e^{ikr'}}{r'}\,da'=\frac{-i\omega\rho}{2\pi}\,u_0e^{-i\omega t}\frac{e^{ikr'}}{r'}\,da'.$$

Therefore

$$p=\mathrm{Re}\int_S dp.$$

The closed form solution for $p$ on the axis of symmetry appears in O'Neil[4] and, in terms of our coordinates, is given by

$$p\begin{bmatrix}x=0\\ t=p\end{bmatrix}=(\rho u_0\omega A/hk)\{\cos\{k[A^2+h^2+2Ah\times(1-a^2/A^2)^{1/2}]^{1/2}\}-\cos[k(A+h)]\}.$$

It is worth reminding the reader here that $h$ can have any value in the range

$$-A\leq h<\infty,$$

where $A>0$. O'Neil obtains this solution by the direct integration over $da'$.

Now we consider the case of a point $Q(x,h)$ in region II. The points in this region can be characterized with the statement that no straight line passing through any one of them and through the center of curvature at (0,0) is at the same time perpendicular to the transducer surface—except for those points on the conical surfaces separating region I from II. Consider the particular field point $Q(x,h)$ in Fig. 2. $Q'$ defines a source point in the $x,h$ plane. The quantity $s$ is the distance from the transducer center of curvature to the field point, $\theta$ is the angle included between $r'$ and $s$, $A$ and $a$ are defined above, $\phi$ equals $\tan^{-1}(x/h)$, and $x_p$ and $z_p$ are Cartesian coordinates having a common origin with the $x,h$ coordinate system and corresponding to the particular value of $\phi$. The dashed line passes through $Q'$ and is perpendicular to the $z_p$ axis. $\hat{n}$ is a unit vector directed from the origin of the coordinate systems toward the transducer surface and is parallel to the axis of symmetry of the transducer. $\psi$ is the angle between $\hat{n}$ and the line connecting the origin (center of curvature) and the source point $Q'$; notice that $\psi$ is positive as shown, but is negative if $Q'$ lies below the axis of symmetry as shown in Fig. 2.

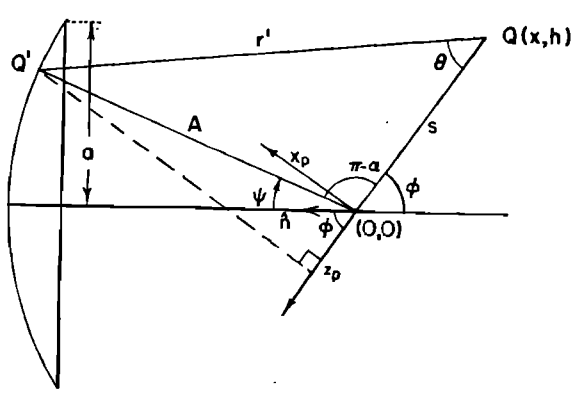


FIG. 2. Diagram including the same plane as in Fig. 1 and illustrating various quantities involved in the theoretical derivation of the pressure field.

Consider the intersection of two spherical surfaces, one of radius $r'$ and centered at $Q(x,h)$ and the other of radius $A$ and centered at $(0,0)$; the latter surface includes the radiating element, of course. This intersection defines a circle lying in a plane passing through $Q'$ and perpendicular to the $z_p$ axis. An arc on this circle lies on the radiating element. Viewed from the point $Q(x,h)$, this arc appears as in Fig. 3—the $z_p$ axis is perpendicular to the page in Fig. 3. The angle defining this arc equals $2\beta$ where $\beta$ is the azimuthal coordinate corresponding to the point $Q''$ where the circle on which the arc lies intersects the edge of the source layer. The radius of the circle including the arc is $r'\sin\theta$ *or* $A\sin(\psi+\phi)$.

Thus the area element on the transducer surface, all the points of which are at the same distance $r'$ from the field point $Q(x,h)$, is given by

$$da' = \underbrace{2\beta A\sin(\psi+\phi)}_{\text{arc length}} A\,d\psi .$$

The angle $\phi$ is constant for fixed $Q(x,h)$; then, defining

$$\alpha \equiv \psi+\phi ,$$

we have $d\alpha = d\psi$ and

$$da' = 2\beta A^2 \sin\alpha\, d\alpha .$$

The limits on $\alpha$ are $\psi_u+\phi$ and $-\psi_u+\phi$. $\beta$, however, is a function of $\alpha$ and corresponds to $r'(\beta)$ in Fig. 3: $r'(\beta)$ is the position vector of $Q''$. But $r'(\beta)\cdot\hat{n} = (A^2-a^2)^{1/2}+h$. We have $r'(\beta) = \hat{i}_p x_p + \hat{j}_p y_p + \hat{k}_p z_p$ where $\hat{i}_p$, $\hat{j}_p$, and $\hat{k}_p$ are the conventional unit vectors in the $x_p$, $y_p$, $z_p$ coordinate system. In terms of spherical polar coordinates referenced to $x_p$ and $z_p$,

$$x_p = r'\sin\theta\cos\beta ,$$

$$z_p = -r'\cos\theta ,$$

and

$$\hat{n} = \sin\phi\,\hat{i}_p + \cos\phi\,\hat{k}_p .$$

Thus

$$r'\cdot\hat{n} = (A^2-a^2)^{1/2}+h = r'\sin\theta\cos\beta\sin\phi - r'\cos\theta\cos\phi .$$

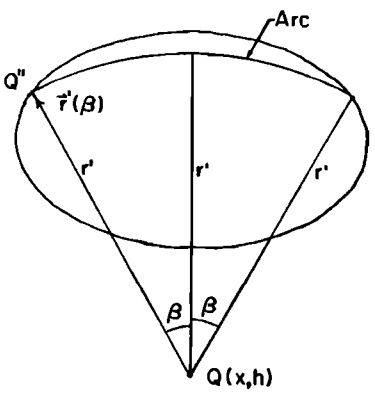


FIG. 3. Diagram of a view of the radiating element in which the $z_p$ axis is perpendicular to—and directed into—the figure (see Fig. 2 for reference). The arc formed by the intersection of a spherical surface of radius $r'$ centered on the field point and that part of the spherical surface defining the radiating element is illustrated. The point $Q''$ is a source point at one end of this arc.

Using the latter relation along with the law of sines, viz.,

$$r'\sin\theta = A\sin(\pi-\alpha) = A\sin\alpha ,$$

and the law of cosines, viz.,

$$A^2 = r'^2 + s^2 - 2r's\cos\theta ,$$

$\beta$ can be written as a function of $r'$ only—or as a function of $u \equiv kr'$ only.

$$\beta = \cos^{-1}\left(\frac{h+(A^2+a^2)^{1/2}-[(u^2/k^2+s^2-A^2)/2s]\cos\phi}{\{u^2/k^2-[(u^2/k^2+s^2-A^2)/2s]^2\}^{1/2}\sin\phi}\right) .$$

The law of cosines also results in

$$r' = [A^2+s^2-2As\cos(\pi-\alpha)]^{1/2}$$

$$= (A^2+s^2+2As\cos\alpha)^{1/2} ,$$

$$u = kr' = (A^2+s^2+2As\cos\alpha)^{1/2} .$$

Changing variables of integration from $\alpha$ to $u$ yields

$$p(t=0) = -\frac{\rho u_0\omega A}{\pi k s}\,\mathrm{Re}\left(i\int_C^D \beta(u)e^{iu}\,du\right) ,$$

where

$$C \equiv k[A^2+s^2+2As\cos(\psi_u+\phi)]^{1/2}$$

and

$$D \equiv k[A^2+s^2+2As\cos(\psi_u-\phi)]^{1/2} .$$

This solution applies whether $h$ is positive or negative.

Region I can be characterized by the fact that for each field point $Q(x,h)$ there exists a straight line through that point which is also perpendicular to the transducer surface. This allows the separation of the transducer surface into two parts, one part consisting of a smaller focused transducer with the same focal point as the larger; this smaller transducer has a projected radius of $A\sin(\psi_u-\phi)$ and its axis of symmetry makes an angle $\phi$ with the axis of symmetry of the transducer face (see Fig. 4). Thus one term in the pressure field can be expressed in closed form using O'Neil's[4] expression for the pressure field on the axis.

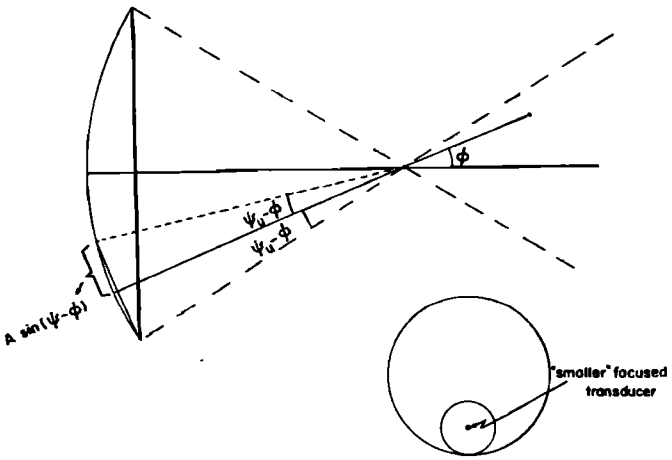


FIG. 4. Diagram showing the source region forming a "smaller" focused transducer discussed in the derivation of the pressure field for region I. This "smaller" focused transducer contributes a closed form (nonintegral) term to the theory.

The contribution of the remaining source area can be represented as a single integral. The analysis is analogous to that done for $Q(x,h)$ lying in region II. We just state the results here. This single integral has exactly the same form as that for region II *including the limits on the integral.*

Summarizing, the pressure at time $t=0$ for any field point in regions I or II is

$$p=-\frac{\rho u_0 \omega A}{\pi k s}\,\mathrm{Re}\left(i\int_C^D \beta(u)e^{iu}\,du+F\right),$$

where $\beta(u)$, $C$, and $D$ are given above, and $F=0$ for region II and

$$F=(\pi|h|/h)(\exp[ik(A+hs/|h|)] - \exp\{ik[A^2+s^2+2As\cos(\psi_u-h\phi/|h|)]^{1/2}\}),$$

for region I. Recall that $h$ can be negative ($-A\le h<\infty$) and that $0\le\phi\le\pi$.

On the axis of symmetry of the transducer ($x=0$) the integral does not contribute, and Re $F$ gives the (O'Neil) answer; however, to avoid difficulties for numerical integrations, the integral should be *set* equal to zero when $x=0$ because, though the limits on the integral become equal for $x=0$, the denominator of $\cos\beta$ goes to zero also.

## II. EXPERIMENTAL MEASUREMENTS

An Aerotech 19-mm, long internal focus, nominal 3.5-MHz transducer was driven with continuous wave (cw) pulse bursts at a frequency of 2.46 MHz, and these generated pulses were received with a Dapco Type NP-10 hydrophone. As is the case for many clinical transducers, the Aerotech source transducer has a "quarter-wave matching layer" attached to the external electrode. Since this layer is only about 0.2-mm thick, it likely has little effect on the pressure field distribution for cw bursts. However, this layer probably has a significant effect on the pulse shape for short pulses such as those used clinically. The quarter-wave layer is in direct contact with the skin during clinical use and in direct contact with the transmitting water in the experiment discussed here.

Figure 5 is a diagram of the apparatus used. The pulse generator controlled the duration and the repetition rate of the cw pulse bursts for sinusoidal signals generated by the gated function generator. The voltage applied to the transducer was kept low enough that conversion of wave energy into higher harmonics due to nonlinear effects during transmission through the water were not detectable. Not only were no deviations from sinusoidal 2.46-MHz wave forms observed on the oscilloscope, but the pressure amplitudes obtained using hydrophone calibration curves were well below those required to yield significant nonlinear effects at the various distances employed[8,9] even if the peak pressure amplitude in the field was assumed to exist at all points in the field.

The source transducer was mounted in a spring-loaded device allowing the direction of the generated beam to be finely adjusted. The receiving Dapco hydrophone was mounted on a Medisonics $x,y,z$ micromanipulator, and the latter was used to move the hydrophone in a plane perpendicular to the beam axis. (We refer to this as the $x,y$ plane henceforth.) Positioning of the hydrophone along the beam axis (henceforth referred to as the $z$ axis) was done primarily by moving the unit consisting of the slider, $x,y,z$ micromanipulator, and hydrophone on the track mounted on the top of the water tank; fine adjustments, however, were performed using the $z$-axis micromanipulator screw.

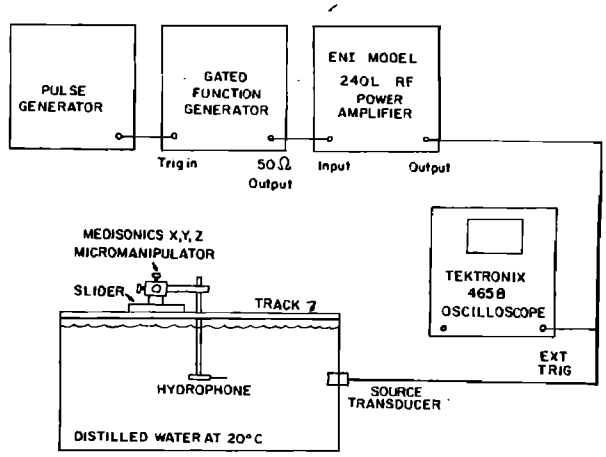


FIG. 5. Diagram of the apparatus used in measuring the amplitudes and phases of the hydrophone response.

The measurement procedure is summarized in the following six steps.

(1) The hydrophone was positioned so that its axis of symmetry was horizontal and passed nearly through the center of the transmitter; also, the receiving tip of the hydrophone was placed at about 4 in. from the center of the transmitter as measured roughly with a ruler. The nominal radius of curvature, given by the manufacturer, was 4 in.

(2) The transmitter, generating cw pulse bursts, was oriented so that the received signal at the hydrophone was maximized.

(3) Deliberate, methodical, successive reorientations of the transmitter's axis of symmetry—along with accompanying appropriate $x,y,z$ translations of the hydrophone—resulted in the determination of an $x,y$ plane in which rings exhibiting zero signal amplitude were present. Given that the transmitter and receiver were axially symmetric, the $z$ axis would then be parallel to the beam axis of symmetry. Perfect axial symmetry is not expected, of course. This $x,y$ plane should be the so-called focal plane defined by $h=0$ in Sec. I. See Secs. III and IV for clarification regarding the expected rings of zero signal amplitude.

(4) The distance between the transmitter and the $x,y$ plane found in (3) was measured by maximizing the signal amplitude (moving the receiving hydrophone piezoelectric element to the beam axis of symmetry), measuring the time passing between the pulse emission and reception, and using the fact that the speed of sound in distilled water at the temperature of the water bath (20°C) was 1482.3°C.[10] This distance, determined in

this fashion, was 11.0±0.1 cm.

(5) The amplitudes and phases of the hydrophone sinusoidal voltage response (receiver signal) were then recorded as functions of position along a straight line in the $x, y$ plane and passing through the point of peak signal amplitude. Such measurements are referred to as determining the "lateral beam profile" for the particular distance between the transmitter and the $x, y$ plane.

(6) Such lateral beam profiles were then measured for a broad range of distances between the transmitter and receiver. The latter distances were determined as in (4) above.

The peak-to-peak amplitudes were measured directly from the waveform displayed on the oscilloscope. The phases were determined by recording the position on the scope screen of any zero voltage (zero crossover) point of the sinusoidal waveform at which point the slope of the waveform was negative. (The zero voltage points at which the slope of the waveform was always positive could also have been employed, of course.) For a given displayed waveform, the difference in phase corresponding to such points is $2\pi n$ rad where $n$ is an integer. Since $e^{i\phi} = e^{i(\phi+2\pi n)}$, such points are equivalent. Since the $z$ coordinates were determined only to within the order of the wavelength at 2.46 MHz, the phases measured at a particular value of $z$ have significant precision only relative to one another. In each of Figs. 6 through 12 the experimentally measured phases have had a constant added to result in agreement between theory and experiment at one lateral position; this lateral position was usually taken to be at the center of symmetry of the lateral beam profile.

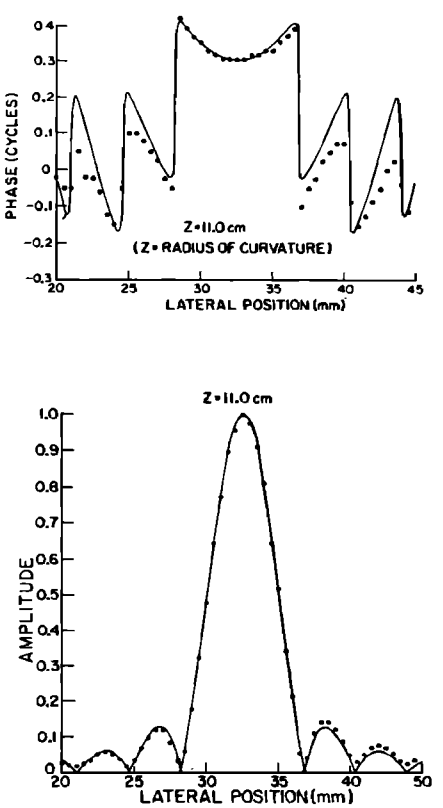


FIG. 6. Phase and amplitude of the hydrophone response as a function of lateral position at an axial distance of 11.0 cm (equal to the radius of curvature) from the radiating element. Theory is shown as smooth lines and experiment as individual data points. The beam axis corresponds to a lateral position of 32.5 mm. The latter point is also at the center of curvature of the radiating element, and at this point—and *only* at this point—the amplitude was normalized to one, both for the theory and for experiment.

## III. RESULTS

The important experimental and theoretical results are displayed in Figs. 6 through 12. Each of these figures corresponds to a fixed specific value of $z$, the distance between the center of symmetry of the lateral beam profile, and the transmitting element. In each figure the amplitude and phase for both theory and ex-

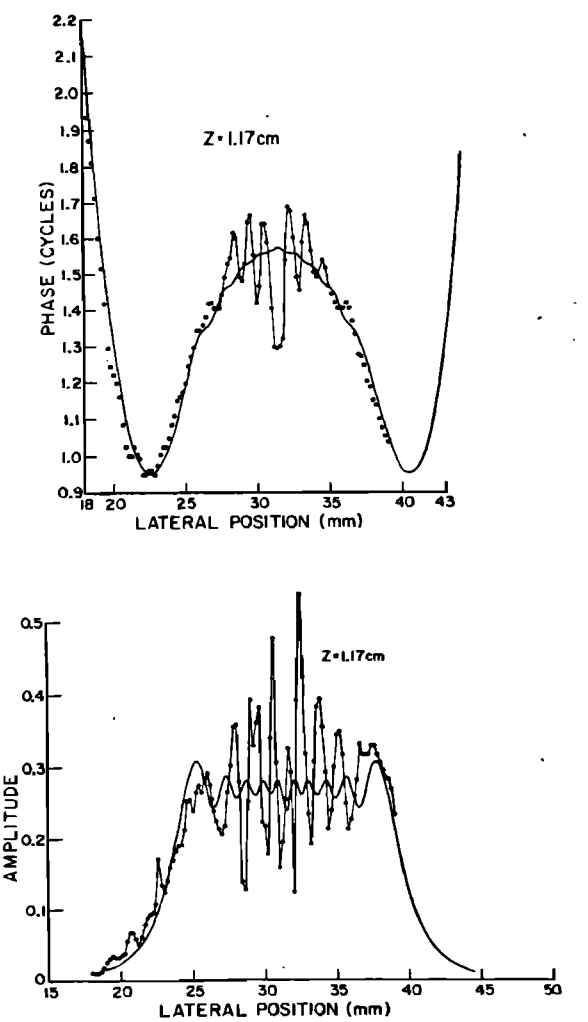


FIG. 7. Phase and amplitude of the hydrophone response as a function of lateral position at an axial distance of 1.17 cm. Theory corresponds to the smooth curved lines and experiment to the individual points; because of the rapid variation with lateral position of the data points in the central region of the beam, adjacent data points have been connected by straight lines as a tracking aid for the eye. The beam axis corresponds to a lateral position of about 31.5 mm. Regarding normalization of the amplitude, for both theory and experiment, see the end of the caption for Fig. 6.

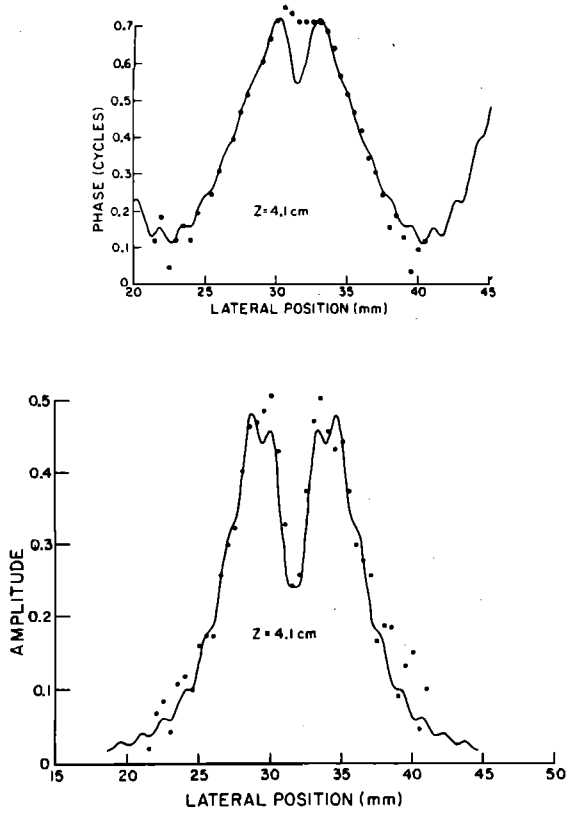


FIG. 8. Phase and amplitude of the hydrophone response as a function of lateral position at an axial distance of 4.1 cm. Theory is shown as smooth lines and experiment as individual data points. The beam axis corresponds to a lateral position of about 31.7 mm. Regarding normalization of the amplitude, for both theory and experiment, see the end of the caption for Fig. 6.

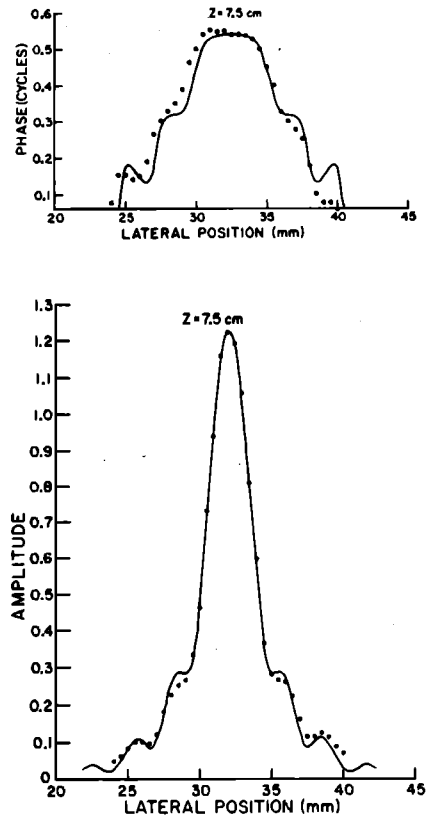


FIG. 9. Phase and amplitude of the hydrophone response as a function of lateral position at an axial distance of 7.5 cm. Theory is shown as smooth lines and experiment as individual data points. The beam axis corresponds to a lateral position of about 32.5 mm. Regarding normalization of the amplitude, for both theory and experiment, see the end of the caption for Fig. 6.

periment are displayed. The continuous smooth curves correspond to theory and the points to experiment. In some of the cases, successive experimental points are connected by straight lines to aid the eye of the viewer in this regard.

Figure 13 shows a plot of the theoretical axial response amplitude (smooth curve) along with six experimental data points for $z = 4.0$, 7.5, 10.0, 11.0, 12.0, and 18.3 cm. The axial response at $z = 1.17$ cm was not plotted because of the difficulty of estimating an appropriate value (see Fig. 7). Figure 13 may be useful to the reader in clarifying the positioning involved in Figs. 6 through 12.

It should be emphasized that the amplitude and phase referred to do not correspond exactly to pressure. In the case of the experimental plots the amplitude and phase of the hydrophone response voltage are plotted. This voltage signal necessarily includes variations from the actual pressure amplitude at a point because of the fact that the hydrophone, although it has a small receiving area (corresponding to a disk of piezoelectric material having a diameter of 1 mm), is not a perfect point receiver. The amplitude of the sinusoidal voltage signal has been normalized to unity at *one point* in the field, viz., at the center of curvature of the piezoelectric element of the focused transmitter. The peak-to-peak voltage amplitude at the center of curvature was 142 mV; thus, all peak-to-peak voltage amplitudes measured (in millivolts) were divided by 142 mV.

The theoretical results correspond to the numerical integration of the pressure (including phase) over the surface of a 1-mm-diam flat circular piston receiver. This results in a force varying sinusoidally in time and this force is assumed to be proportional to the voltage observed across the terminals of the hydrophone. A normalizing constant has been introduced requiring the amplitude of this force to be unity at the center of curvature of the transmitter. The amplitude and phase of this normalized force appear in Figs. 6 through 12, and only the amplitude appears in Fig. 13.

According to O'Neil[4] (see particularly p. 521, 525, and 526) the pressure amplitude in the "focal plane" should be very nearly proportional to the farfield directivity function for a flat circular piston, i.e.,

$$\text{pressure amplitude } \bar{\alpha}\,(2/z)J_1(z),$$

for

$$z = ka \sin\theta .$$

In this expression $k$ is the wavenumber, $a$ is the radius of the circle defining the outer edge of the radiator, and

$$\sin\theta = x/(A^2+x^2)^{1/2},$$

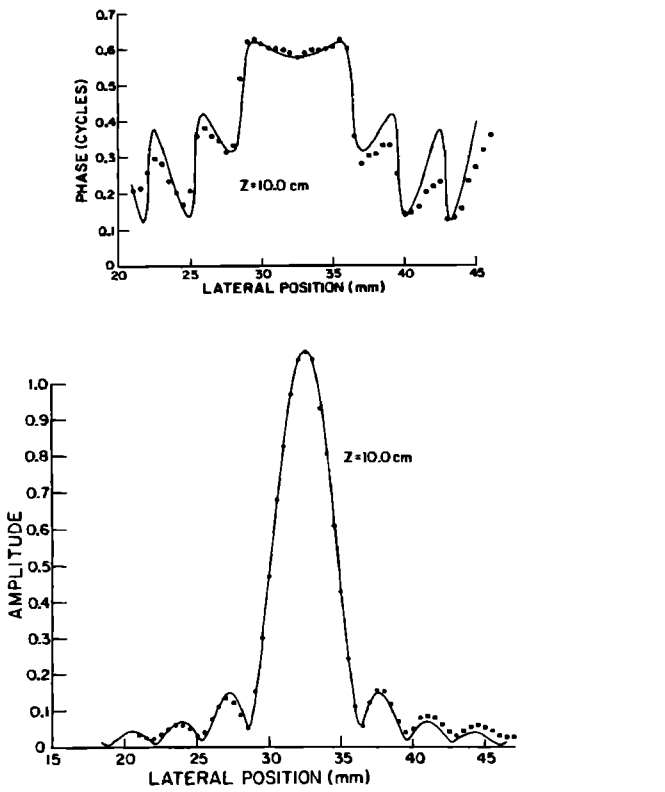


FIG. 10. Phase and amplitude of the hydrophone response as a function of lateral position at an axial distance of 10.0 cm. Theory is shown as smooth lines and experiment as individual data points. The beam axis corresponds to a lateral position of about 32.5 mm. Regarding normalization of the amplitude, for both theory and experiment, see the end of the caption for Fig. 6.

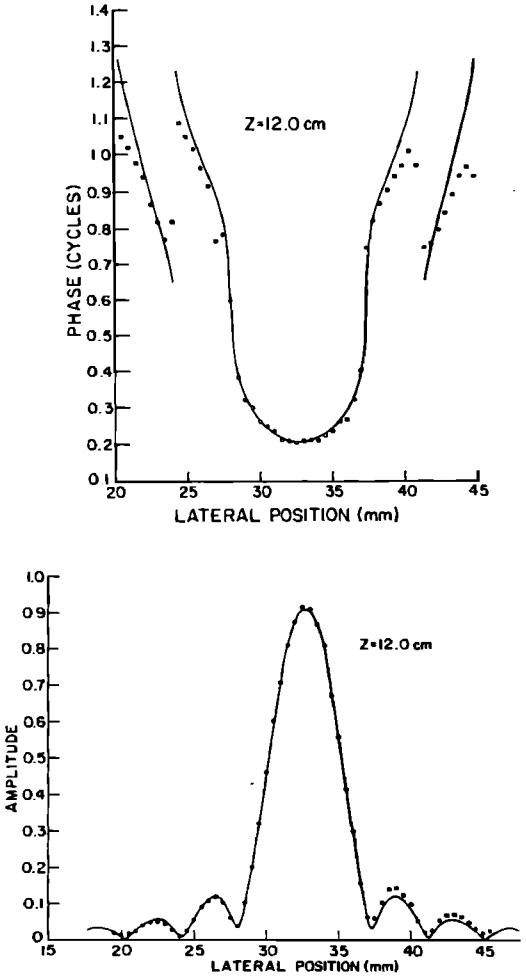


FIG. 11. Phase and amplitude of the hydrophone response as a function of lateral position at an axial distance of 12.0 cm. Theory is shown as smooth lines and experiment as individual data points. The beam axis corresponds to a lateral position of about 32.7 mm. Regarding normalization of the amplitude, for both theory and experiment, see the end of the caption for Fig. 6.

where $x$ and $A$ were defined in the theory section of this paper. The "focal plane" refers to a plane perpendicular to the beam axis of symmetry and including the center of curvature of the radiating element. The pressure amplitude in the focal plane obtained with the theory described in this paper corroborates O'Neil's statement. Computer printouts of $(2/z)J_1(z)$ and the result of the theory presented above were indistinguishable.

Figure 6 shows relative amplitude versus position on a line in the focal plane passing through the beam axis of symmetry. The positions are values read from a vernier on the $x,y,z$ micromanipulator. The smooth curve is the result of theory, and the points correspond to experimental measurements. Excellent agreement between theory and experiment is apparent particularly for the smaller values of the position coordinates. The zero values of the amplitudes adjacent to the central peak were very sharply defined experimentally: relative to translation parallel to the beam axis (perpendicular to the focal plane) they determined to within ±1 mm. This includes a resolution of about 0.1 mV for the peak-to-peak amplitude on the oscilloscope.

This agreement between our theory, O'Neil's theory, and experiment leads to the conclusion that the focal plane—or plane passing through the center of curvature of the focused radiator—had been determined experimentally by finding these points of zero amplitude (see step 3 of the measurement procedure in Sec. II). The radius of curvature determined in this way was 11.0 ±0.1 cm. This does not agree very well with the nominal 4 in. ≃10.2-cm radius of curvature specified by the manufacturer. We believe our value is closest to the correct one, however; this is a subject in Sec. IV. The radius of curvature in the theory was taken to be that determined ultrasonically, viz., 11.0 cm and the diameter of the transducer was taken to be 19 mm.

The values of $z$ selected for the measurements span the range over which a "contact" transducer would be employed in diagnostic imaging. In addition to 11.0 cm, the radius of curvature of the transmitter, these are 1.17, 4.1, 7.5, 10.0, 12.0, and 18.3 cm. The latter six values correspond to Figs. 7 through 12, respectively. Three of these values cover the region of the center of curvature of the transmitter (10.0, 11.0, and 12.0 cm). The value $z=7.5$ cm defines a plane containing the peak pressure amplitude for the 2.46-MHz frequency.

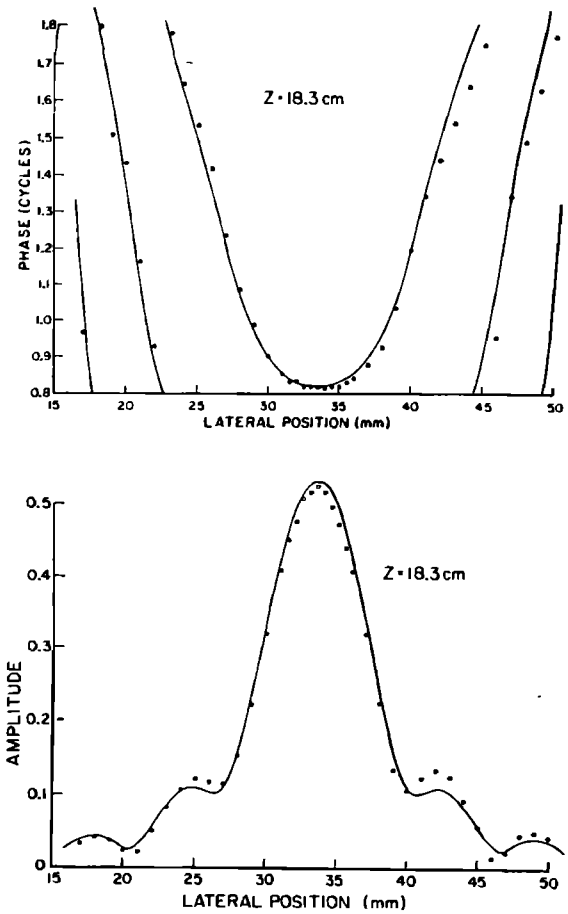


FIG. 12. Phase and amplitude of the hydrophone response as a function of lateral position at an axial distance of 18.3 cm. Theory is shown as smooth lines and experiment as individual data points. The beam axis corresponds to a lateral position of about 33.5 mm. Regarding normalization of the amplitude, for both theory and experiment, see the end of the caption for Fig. 6.

## IV. DISCUSSION

### A. Experimental errors

The precision of the measurements in this experiment was probably determined primarily by the experimenters' ability to read the oscilloscope trace and the vernier of the $x, y, z$ manipulator. The Tektronix 465 B scope has a screen with ten divisions vertically and horizontally. The sweep rate was maintained at 0.1 $\mu$s/div throughout the experiment except when values of $z$ were determined via time of flight. Assuming that the zero crossover points employed in measuring phase were determined within $\pm 0.05$ oscilloscope divisions, this means that the phases were determined within $\pm 0.05/4 \simeq \pm 0.01$ cycles. (There are about four divisions per cycle at 2.46 MHz and 0.1 $\mu$s/div.) The degree of smoothness of the experimental phase plots is consistent with this estimation of precision.

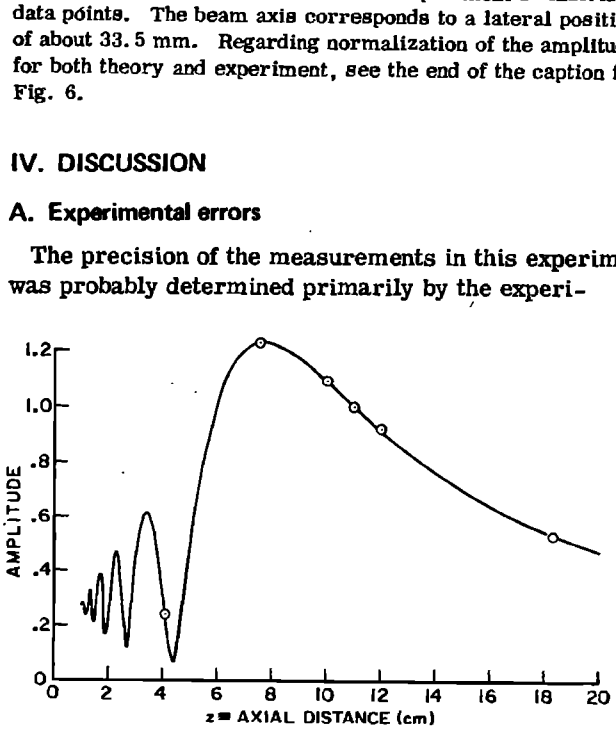


FIG. 13. Response amplitude along the transmitting transducer's axis of symmetry. The smooth curve corresponds to theory and the circled points correspond to experimental measurements. See Figs. 6 and 8–12 for experimental values at $z = 11.0$, 4.1, 7.5, 10.0, 12.0, and 18.3, respectively.

In measuring the distances, $z$, between the transmitter and receiver, the latter being on the beam axis of symmetry, a typical number of oscilloscope divisions between the displayed transmitted pulse and the received pulse was about six. Again assuming that the scope could be read to within about $\pm 0.05$ divisions, this corresponds to an error in $z$ determinations of $\pm 1\%$. Thus, e.g., the distance from the center of the transmitter to the focal plane is $11.0 \pm 0.1$ cm.

The measurement of peak-to-peak voltage amplitudes was, as in the case of the phase and $z$ distance determinations, limited by the experimenters' ability to read the scope trace. Typically the peak-to-peak measurement was about six vertical divisions. Again assuming an error of $\pm 0.05$ divisions, this yields a precision of $(0.05/6) \times 100 = 1\%$. As in the case of the phases, the degree of smoothness of the amplitude plots indicates this to be a good estimate of precision.

That the above estimates of precision also are representative of the accuracy is supported by the facts that vertical calibration of the oscilloscope was carried out only two months before the experiment and that sweep rate calibration was done at the time of the experiment using a 4.27000-MHz crystal oscillator circuit.

### B. Comparison of theory and experiment

Theory and experiment agree very well for all values of $z$ other than 1.17 cm. Slight asymmetry in the experimental lateral beam profiles exists and agreement between theory and experiment tends to be better on the left sides of the graphs in Figs. 6 through 12. Consider the amplitude graphs first.

Even at 4.1 cm (Fig. 8), where a sharp minimum in the amplitude is seen in both theory and experiment, agreement is good. Two relative maxima present themselves between 1 and 4 mm from the central minimum. The greater maximum is that closest to the central minimum in the experimental case and is that furthest from the central maximum in the case of theory. The overall relative values, however, agree very well. For all values of $z$ other than 1.17 cm, the axial values show excellent agreement; comparison in the focal plane ($z = 11.0$ cm) is excluded from this observation, of course, since both theory and experiment were both normalized to unity there.

For $z = 1.17$ cm (Fig. 7), relatively violent fluctuations in amplitude as a function of position were ob-

served experimentally. Fluctuations in the theory are also present but are very much subdued in comparison. Weight and Hayman[11] have suggested that radial modes of oscillation may account for this phenomenon for circular flat piston transmitters. An analogous situation may exist for this case.

The same type of more extensive fluctuation in phase is observed experimentally rather than theoretically at 1.17 cm. At 4.1 cm (Fig. 8) the central minimum in phase described by the theory might be considered to have been demonstrated experimentally on the left side of the graph. In the remaining graphs of phase (Figs. 6 and 9–12) fluctuations near amplitude minima are more subdued experimentally than theoretically.

It is emphasized that the theoretical results presume that the receiver is a flat circular piston receiver having a diameter of 1 mm. That this is a reasonable model for the hydrophone is supported by the degree of correspondence between theory and experiment.

The value for the radius of curvature used in the theory was 11.0 cm which was determined by finding that plane in which the directivity function was observed, including zeros adjacent to the central peak. This value was found independently on four occasions by executing item (3) described in Sec. II. This value is about 8 mm greater than the nominal value quoted by the transducer manufacturer who receive their piezoelectric elements from another manufacturer. We feel that our value is the correct one because the technique of determining the plane exhibiting the directivity function has yielded good agreement with the manufacturers' specified radii of curvature on two other transducers, one of them being another focused Aerotech transmitter. Our values were 13.7 and 6.35 cm and the corresponding manufacturers' values were $14.0 \pm 0.3$ cm and 6.50 cm, respectively; our values in these cases were actually about 2% below the manufacturers' values. A direct measurement of the radius of curvature of the outer surface of the "quarter-wave" layer on the transducer used in our experiment yielded $10.6 \pm 0.3$ cm. The 11.0-cm value obtained for us by the transmitting element is likely the best value to be found short of destructive testing methods.

### C. Measurements on other transducers

Limited measurements were done on two other focused clinical transducers and theory compared with experiment. One of these was another Aerotech transducer with a specified diameter of 19 mm, a radius of curvature of $14.0 \pm 0.3$ cm, and nominal frequency of 2.25 MHz. Measurements of amplitude and phase were made only in the focal plane where the directivity function is expected to apply (corresponding to Fig. 6). Agreement between theory and experiment was slightly better for this transducer than that shown in Fig. 6; this is because the approximately 10% disagreement on the right side of the amplitude peak was absent.

The other transducer tested had a manufacturer's specified radius of curvature of 6.5 cm and a diameter of 3 cm. Thus the ratio $A/a$ was about 4.3 as opposed to about 12.5 for the transducer reported. The agreement between theory and experiment was good but not as good for this transducer as for the one reported. The data for this transducer were not reported here because it was discovered that the amplitudes observed were too large to exclude significant transfer of wave energy to higher harmonics during transmission through the water.[8,9] The results are more appropriate for inclusion in a future paper involving nonlinear effects.

### D. Attenuated pulse generation using continuous wave theory

The solution for the spatial dependence of the pressure field generated by a transducer consisting of a spherical shell transmitter the outer edge of which is a circle was described in the theory section for the case in which the Rayleigh formula is valid. This implies that a uniform distribution of identical point sources exists over the surface of the transmitting element. These point sources all generate sinusoidal (cw) spherical waves of the same amplitude and phase. For the boundary conditions corresponding to the Rayleigh formula the beam pattern generated by evaluating the Rayleigh formula is the solution of the Helmholtz equation.

If these point sources emit identical spherical wave pulses, instead of continuous waves, then these pulses are linear superpositions of the cw spherical waves. This can be shown using the completeness of Fourier integration. As a result, the solution of the Helmholtz equation for the spatial and time dependence of such a pulsed beam (created by all the pulsed point sources) can be expressed as a linear superposition of the cw solutions, the coefficients of superposition being determinable via Fourier analysis. Because of the real nature of the pressure pulse, only the cw beam solutions for positive (or negative) values of $\omega$ are needed for completeness. In equation form this means we can write the position and time dependence of a pressure pulse, $p(\mathbf{r},t)$ as

$$p(\mathbf{r},t) = \mathrm{Re}\int_0^\infty A_0(\omega)P_N(\omega,\mathbf{r})e^{-i\omega t}\,d\omega,$$

where $P_N(\omega,\mathbf{r})e^{-i\omega t}$ is the normalized complex cw pressure beam corresponding to the angular frequency, $\omega$, the spatial position, $\mathbf{r}$, and time, $t$. $A_0(\omega)$ is the complex superposition coefficient which can be determined using Fourier analysis if $p(\mathbf{r},t)$ is known at a single point $\mathbf{r}_0$. The functions $P_N(\omega,\mathbf{r})$ can be normalized in any way; e.g., one could require $P_N(\omega,\mathbf{r}_c)=1$ where $\mathbf{r}_c$ is the position vector of the center of curvature of the focused transducer. To include the effects of attenuation on such a pulse, recall that the theory includes the wavenumber $k=k(\omega)$. With no attenuation $k=\omega/c$ where $c$ is the constant speed of sound. With nonzero attenuation, and allowing a frequency dependence of the speed of sound, $k$ becomes complex as follows:

$$k(\omega) = [\omega/c(\omega)] + i\alpha(\omega),$$

where $c(\omega)$ is the (real) frequency dependent speed of sound and $\alpha(\omega)$ is the (real) frequency dependent atten-

uation coefficient in nepers per unit length. Thus attenuation and dispersion during transmission through a medium is accounted for in the integral expression for $p(\mathbf{r},t)$ above if this complex $k(\omega)$ is introduced into $P_N(\omega,\mathbf{r})$ in the integrand.

## V. CONCLUSIONS

The precise experimental measurements of the cw pulse burst pressure field for a clinical focused transducer displayed in Figs. 6 through 12 are of considerable value for testing theoretical calculations of such pressure fields. Extensive agreement was found between experiment and theory, the latter being in the form of the Rayleigh formula. This agreement broke down in the field very near to the transmitting element; thus more work remains to overcome this discrepancy.

The Rayleigh formula contains a double integral corresponding to integration over the surface of the transmitting element. In the theoretical section of this paper the reduction of the double integral to a single integral is described. This results in considerable reduction in computer time for the performance of precise integrations numerically. This time saving is valuable particularly when formation of broadband pulses via superposition of cw solutions is done. Formation of such pulses as functions of time and position, both in attenuating and nonattenuating media, is the subject of another paper.[6] In the latter, theory and experiment again are compared.


## ACKNOWLEDGMENTS

Our work was supported by NCI grants 5-R01-CA25634, 5-P01-CA19278, and 5-T32-CA09206. The figures were generated by Orlando Canto and the manuscript typed by Kathryn McSherry and Anne Zimmerman.



[1]P. R. Stepanishen, J. Acoust. Soc. Am. 49, 841–849 (1971).

[2]J. C. Lockwood and J. G. Willette, J. Acoust. Soc. Am. 53, 735–741 (1973).

[3]G. Kossoff, Ultrasound Med. Biol. 5, 359–365 (1979).

[4]H. T. O'Neil, J. Acoust. Soc. Am. 21, 516–526 (1949).

[5]A. Penttinen and M. Luukkala, J. Phys. D: Appl. Phys. 9, 1547–1557 (1976).

[6]M. M. Goodsitt, E. L. Madsen, and J. A. Zagzebski, "Field patterns of pulsed focused ultrasonic radiators in attenuating and nonattenuating media," J. Acoust. Soc. Am. (submitted for publication).

[7]P. M. Morse and K. U. Ingard, *Theoretical Acoustics* (McGraw-Hill, New York, 1968).

[8]T. G. Muir and E. L. Carstensen, Ultrasound Med. Biol. 6, 345–357 (1980).

[9]E. L. Carstensen, W. K. Law, N. D. McKay, and T. G. Muir, Ultrasound Med. Biol. 6, 359–368 (1980).

[10]V. A. Del Grosso and C. W. Mader, J. Acoust. Soc. Am. 52, 1442–1446 (1972).

[11]J. P. Weight and A. J. Hayman, J. Acoust. Soc. Am. 63, 396–404 (1978).